## PAPER

Check for updates

# Machine learning-based correction for spin–orbit coupling effects in NMR chemical shift calculations†

Julius B. Kleine Büning, [ID] [a] Stefan Grimme [ID] *[a] and Markus Bursch [ID] *[b]

As one of the most powerful analytical methods for molecular and solid-state structure elucidation, NMR spectroscopy is an integral part of chemical laboratories associated with a great research interest in its computational simulation. Particularly when heavy atoms are present, a relativistic treatment is essential in the calculations as these influence also the nearby light atoms. In this work, we present a $\Delta$-machine learning method that approximates the contribution to $^{13}C$ and $^1H$ NMR chemical shifts that stems from spin–orbit (SO) coupling effects. It is built on computed reference data at the spin–orbit zeroth-order regular approximation (ZORA) DFT level for a set of 6388 structures with 38 740 $^{13}C$ and 64 436 $^1H$ NMR chemical shifts. The scope of the methods covers the 17 most important heavy p-block elements that exhibit heavy atom on the light atom (HALA) effects to covalently bound carbon or hydrogen atoms. Evaluated on the test data set, the approach is able to recover roughly 85% of the SO contribution for $^{13}C$ and 70% for $^1H$ from a scalar-relativistic PBE0/ZORA-def2-TZVP calculation at virtually no extra computational costs. Moreover, the method is transferable to other baseline DFT methods even without retraining the model and performs well for realistic organotin and -lead compounds. Finally, we show that using a combination of the new approach with our previous $\Delta$-ML method for correlation contributions to NMR chemical shifts, the mean absolute NMR shift deviations from non-relativistic DFT calculations to experimental values can be halved.

## 1 Introduction

Nuclear magnetic resonance (NMR) spectroscopy is a highly valuable analytic tool for structure elucidation and has become a standard method that is used on a daily basis throughout various chemical disciplines.[1–3] Besides experimental analysis, the computation of NMR parameters can further yield detailed insight into chemical phenomena and complex bonding situations. In particular, density functional theory (DFT) has proven to be a reliable and efficient choice for the calculation of NMR parameters.[4–12] Nevertheless, the complex physical relationship between these parameters, the electronic structure, and the chemical environment of the investigated compound remains challenging for quantum chemical methods.[13–15]

There are five main sources of error in quantum chemical NMR prediction as claimed by Lodewyk *et al.*,[13] which are

electron correlation, solvation effects, conformational flexibility, rotational-vibrational, and relativistic effects. The latter become specifically relevant when NMR properties of heavy elements (which we refer to as having an atomic number larger than 18 and including Cl) are computed or if such elements are present in close vicinity to the nucleus under consideration. Heavy elements can play major roles in various application areas, including catalysis,[16–18] batteries,[19,20] and optoelectronics.[21,22] Furthermore, there is a great research interest in biology and biochemistry due to the toxicity of some heavy elements (*e.g.*, Ni, Cd, Hg, Pb)[23] or their essential role in biochemical processes, as for Zn[24–26] and Se.[27–29]

The most crucial relativistic effects originate from spin–orbit (SO) coupling and can be essential even for qualitative modeling of the heavy atom (HA) itself,[11,30,31] but also for the adjacent lighter atoms by the heavy atom on the light atom (HALA) effect.[10,32,33] There are several physics-based methods to incorporate relativistic effects into quantum chemical calculations such as the Douglas–Kroll–Hess (DKH)[34,35] method, the exact transformation of the four-component Dirac equation to two components (X2C),[36–38] and the zeroth-order regular approximation (ZORA).[39,40] However, the spin–orbit variants of these methods in combination with NMR shielding tensor calculations typically

*[a] Mulliken Center for Theoretical Chemistry, Clausius Institute for Physical and Theoretical Chemistry, University of Bonn, Beringstr. 4, 53115 Bonn, Germany. E-mail: grimme@thch.uni-bonn.de*

*[b] Max-Planck-Institut für Kohlenforschung, Kaiser-Wilhelm-Platz 1, 45470 Mülheim an der Ruhr, Germany. E-mail: bursch@kofo.mpg.de*

† Electronic supplementary information (ESI) available. See DOI: https://doi.org/10.1039/d3cp05556f

become computationally unfeasible for larger compounds due to their high computational demand. Further, such methods are not available in many chemical software packages. Accordingly, more efficient and easily accessible methods to include SO-relativistic effects in the calculation of NMR parameters are highly desirable. Such effects are typically neglected in most low-cost approaches, as done in a recently published correction scheme for efficient NMR chemical shielding prediction[41] and a study on halogenated natural products.[42]

One approach to solve this issue and fill this methodological gap can be an empirical model based on machine learning (ML). The field of ML in chemistry has evolved rapidly in the past decade and besides approaches that tackle the complete electronic structure of a quantum chemical system,[43–45] several techniques for the calculation of NMR chemical shifts have been developed.[46–48] Especially for NMR-aided structure assignment, the popular DP4 method[49] was improved with an ML approach called DP4-AI[50] and an ML-based technique for structure assignment from two-dimensional NMR spectra has been proposed.[51] ML approaches can exploit their full potential for highly accurate predictions if they are combined with DFT and use features from a converged electronic structure as input (Δ-ML). This has been shown to yield highly accurate electronic energies[52] and NMR chemical shifts[53–56] at costs not significantly higher than for the underlying low-level method.

There is evidence that in order to achieve a good prediction quality for $^{13}$C NMR chemical shifts of carbon atoms attached to heavy atoms, it is important to account for both correlation and heavy atom effects.[13,57,58] In a test on the $o$-bromochlorobenzene molecule,[59] the pragmatic combination of a non-relativistic second-order Møller–Plesset perturbation theory (MP2) calculation and a SO contribution calculated with DFT yielded the best results compared to experimental data and was the only tested method to achieve a qualitatively correct chemical shift ordering of the six $^{13}$C nuclei. We are therefore confident that a combination of separate correlation and spin–orbit corrections will be beneficial for the efficient computation of reasonably accurate NMR chemical shifts. We previously proposed an ML-based correction method that obtains the (beyond DFT) correlation contribution to NMR chemical shifts based on coupled cluster (CCSD(T)) reference data,[55] which we now call $\Delta_{corr}$-ML. In this work, we present an efficient and highly transferable approach called $\Delta_{SO}$-ML to compute the spin–orbit relativistic contribution to $^{13}$C and $^{1}$H NMR chemical shifts. This new approach is validated for a large number of unique chemical shifts computed at the SO-ZORA-DFT level and is exemplarily applied to $^{13}$C NMR chemical shifts in experimentally accessible organotin and -lead compounds and in a set of heavy metal–organic compounds with experimental reference data.

## 2 Methods

### 2.1 Machine learning data set

As in our previous work on the correction of $^{1}$H and $^{13}$C NMR chemical shifts using machine learning,[55] quantum chemical

*ab initio* data serve as target for the model presented herein. The use of experimental data would increase the overall complexity thus making the data set less suitable for applying an ML correction procedure. Furthermore, the target was chosen such that it keeps an unadulterated focus on one specific component of the chemical shielding constant calculation, spin–orbit coupling. A clear distinction of SO effects from various other error sources in experimental data would be impossible and such an approach would prevent a targeted elimination of the SO error.

The data set is one of the central parts in every ML model and is often particularly challenging to compile for ML applications in chemistry when reference data is sparse. Since it is largely responsible for the performance of the model, we focus on the most common bonding situations in classical (metal-)organic compounds. Further, a focus is set on heavy non-radioactive elements of groups 12 to 17. This includes most p-block elements except for noble gasses and group 12 transition metals as their chemistry is comparably dominated by p-orbitals.[33] As NMR parameters tend to be spatially local, the reference molecules can be chosen rather small (3–46 atoms). This allows for the inclusion of many different bonding motifs, covering a wide chemical space with a sufficiently large amount of samples. The data set consists of 1597 unique molecules, in which at least one heavy atom ($Z \geq 17$) is covalently bound to a carbon atom. These molecules were created manually, starting with the methyl compounds mentioned in Section 3.3.1, and subsequent substitution of the ligands with larger aliphatic, aromatic, and functional residues that are typically found in compounds of the respective heavy element. Analogous structures are included for all elements within the same group and some more complex compounds were added. The structures were selected such that they are chemically reasonable, yet they do not have to be accessible in an experimental setting. To enrich the data, three geometrically distorted structures, one out of each energy window of 2.5–5.0 kcal mol$^{-1}$, 10.0–15.0 kcal mol$^{-1}$, and 30.0–40.0 kcal mol$^{-1}$ above the optimized structures (at the r$^2$SCAN-3c[60] level) were added (for more information on the distortion procedure, see ref. 55 and the ESI†). The overall 6388 structures include data points for 38 740 $^{13}$C and 64 436 $^{1}$H NMR chemical shifts, which is illustrated in Fig. 1. The set includes 2264 structures containing Cl, Br, or I; 1440 structures containing Se or Te; 1260 structures containing As, Sb, or Bi; 1680 structures containing Ge, Sn, or Pb; 804 structures containing Ga, In, or Tl; and 868 structures containing Zn, Cd, or Hg.

### 2.2 Reference level of theory

The target of the $\Delta_{SO}$-ML approach presented here is the contribution to the chemical shielding constant that originates from the inclusion of spin–orbit relativistic effects with a suitable computational method. Scalar-relativistic approaches that either employ effective core potentials (ECPs) or explicitly use a scalar-relativistic (SR) Hamiltonian are available in many quantum chemical program packages such as ORCA. As all-electron approaches with SR-Hamiltonian can be regarded the

This journal is © the Owner Societies 2024

*Phys. Chem. Chem. Phys.*, 2024, **26**, 4870–4884 | **4871**

**Fig. 1** Key specifications of the data set. Included heavy elements are marked in yellow followed by the number of structures that contain them.

more general and reliable choice for the calculation of properties with relevant nucleus effects, we chose an efficient all-electron SR-DFT calculation as origin of the ML input features to predict the additive spin–orbit (SO) correction with our $\Delta_{SO}$-ML model. This contribution $\Delta_{SO}\delta$ is calculated from chemical shifts $\delta$ obtained by including the different levels of relativity:

$$\Delta_{SO}\delta = \delta_{SO} - \delta_{SR}. \tag{1}$$

In this work, we determine the target $\Delta_{SO}\delta$ from two-component SR/SO-ZORA (zeroth-order regular approximation) calculations at the PBE0[61,62] hybrid DFT level of theory with the Slater-type triple-$\zeta$ TZ2P[63] basis set. Note that the performance of an ML approach is directly influenced and limited by the quality – especially the noisiness – of the reference data.[64] PBE0 is a generally robust functional that usually yields good NMR properties and especially the SO-relativistic variant has proven reliable performance in our previous studies on $^{29}$Si[10] and $^{119}$Sn[11] NMR chemical shifts. Furthermore, in contrast to full four-component relativistic methods, SO-ZORA-PBE0 is still feasible for the medium-sized ($>$40 atoms) molecules included in the data set. The transferability of our approach based on the PBE0/TZ2P data to other density functionals and basis sets is further discussed in Section 3.3.1.

To make it easily accessible, the presented method is built onto a scalar-relativistic baseline level of theory calculated using Gaussian-type orbitals with the ORCA program package (although it is in principle not limited to it). The SR-PBE0/ZORA-def2-TZVP level of theory serves as low-level method for most evaluations shown below.

### 2.3 Neural network architecture and input feature vector

With the data set and the target values $\Delta_{SO}\delta$ at hand, an ML model can be constructed. For this purpose, the data set is randomly divided into a training set to build the model and a test set that serves as basis for all evaluations made in Section 3. The data is processed in an atom-wise fashion but it is ensured that all atoms from an individual structure are attributed to the same data set (shuffling mode structures, see ESI,† Section 2.2 for details). Data from a sample molecule and its low-level NMR shielding calculation (currently only possible *via* the ORCA 5 program package) can finally be used to predict $\Delta_{SO}\delta$. The complete workflow is illustrated in Fig. 2.
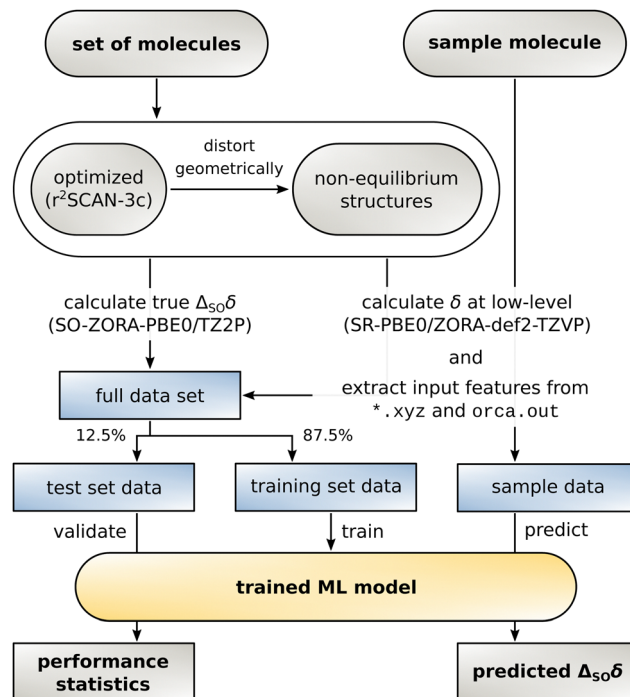


**Fig. 2** Workflow of the $\Delta_{SO}$-ML method used in this work. A set of organic molecules with heavy elements is structurally optimized and geometrically distorted structures are created. For these, reference and low-level data are calculated, from which input features are extracted that make up the data set. 7/8 of the data set are used to train the ML model, 1/8 for validation. For a sample molecule, $\Delta_{SO}\delta$ can then be predicted by the model from the low-level data.

The regression artificial neural network used herein is similar to the one used for our previous $\Delta_{corr}$-ML model for correlation contributions of the chemical shift.[55] The same multilayer perceptron architecture with two hidden layers was used in TensorFlow 2.12 and the input feature vector was modified to adapt it to the SO contribution problem. After initial testing, the hyperparameters were set to 300/12 nodes for the first/second hidden layer for $^{13}$C (384/80 for $^1$H) with a dropout rate of 0.1 for the first layer for $^{13}$C (0.15 on first and 0.1 on second layer for $^1$H) and the adam optimizer. The activation function on all layers was set to GELU (Gaussian Error Linear Unit) for $^{13}$C and the sigmoid function was used for $^1$H. The distribution of the SO contribution values to the chemical shift in the data set is very heterogeneous. Most of the atoms are not in direct vicinity to a heavy atom, so $\Delta_{SO}\delta$ is small but few atoms exhibit a very large value. To make the model focus on the important large values while not placing too much weight on unaffected atoms, the root mean squared deviation (RMSD) was chosen as loss function and showed to be superior to the mean absolute deviation (MAD) and the mean squared deviation (MSD). For the same reason, the RMSD is suited better than the MAD for the evaluations below.

The information included as input is of central importance for the quality and performance of the ML model.[64] In the case of $\Delta_{SO}$-ML, the input feature vector is constructed such that it contains information about the geometric (solely from the

**4872** | *Phys. Chem. Chem. Phys.*, 2024, **26**, 4870–4884

This journal is © the Owner Societies 2024

three-dimensional structure), electronic (from the converged density matrix of the DFT single-point calculation), and magnetic (from the DFT NMR shielding constant calculation) surrounding of each atom of interest. The majority of the descriptors of these categories was taken from the $\Delta_{corr}$-ML model and some were omitted. A set of atom-centered symmetry functions[65] (ACSF) was further added.

Furthermore, a new range of descriptors was added that contains geometric and electronic information about heavy atoms in the vicinity of the atom of interest. These include:

• The total number of heavy atoms bound to the nucleus of interest *via* one to five covalent bonds,

• The average atomic mass of all atoms within one to five covalent bonds,

• The atomic number of the heavy atom(s),

• The coordination number (from the D3 model) of the heavy atom(s), and

• The atomic, and s-, p-, and d-orbital Mulliken populations of the heavy atom.

The latter ones are arranged in sets of five descriptors per heavy atom in the first covalent bond shell. The inclusion of the atomic charge and the s- and p-orbital populations was motivated by the findings of Vícha *et al.* on the spin–orbit heavy-atom (HA) effect on the light atom (LA).[33] These suggest that for most heavy elements the chemical shift contribution originating from spin–orbit coupling has a fixed sign. Accordingly, the HA effect on the LA is always shielding or deshielding (this information is covered by the atomic number of the HA). The cause of this trend lies in the electronic configuration, as formally empty valences shells of the HA (*e.g.*, $p^0$, $d^0$) typically lead to a deshielding mechanism whereas partially filled sub-shells (*e.g.*, $p^2$, $p^4$) result in a shielding effect. In some cases, however, different contributions occur simultaneously with comparable magnitudes so that the sign of $\Delta_{SO}\delta$ may vary, *e.g.*, depending on the oxidation state of the HA. Therefore, the atomic charge and orbital populations of the HA are included as descriptors. A detailed list of the complete input feature vector is provided in the ESI,† Table S2.

### 2.4 Computational details

The compounds in the data set were chosen and created manually and a selected structure was pre-optimized at the semiempirical tight-binding GFN2-xTB[66] level using the xtb 6.6.0[67] program package. Subsequent geometry optimizations where performed with the TURBOMOLE 7.7.1[68–70] program package using the r²SCAN-3c[60,71,72] composite DFT method. Throughout the geometry optimizations, the resolution of the identity approach for Coulomb integrals (RIJ)[73] was applied and the m4 grid and a radial grid size of 10 were used. For the tests on the experimentally accessible structures in Sections 3.4.2 and 3.4.3, conformer ensembles were generated using the conformer-rotamer ensemble sampling tool (CREST),[74,75] version 2.12, using the GFN-FF[76] force field and GFN2-xTB with the ALPB[77] solvation model (solvent as in the experimental measurement). The ensembles were further refined with the command-line energetic sorting (CENSO)[78,79] algorithm,

version 1.2.0, at the final level r²SCAN-3c + $G_{solv}$(COSMO-RS)[80–82] + $G_{mRRHO}$(GFN2-xTB)[83–85]//r²SCAN-3c(DCOSMO-RS).[86]

All NMR shielding constant calculations in this study were performed *via* the gauge-including atomic orbital (GIAO)[87–89] approach using the ORCA 5.0.4[90–92] program package for calculations with Gaussian-type orbital (GTO) basis sets and the ADF module of the AMS 2022.103[93] program package for Slater-type orbital (STO) basis sets. For the low-level shielding calculations (ORCA), the Hamiltonian of the scalar-relativistic (SR) zeroth-order regular approximation (ZORA)[39,94] was used in combination with the PBE[95] general gradient approximation (GGA) and the PBE0[61] and r²SCAN0[96] hybrid density functionals, together with the GTO triple-ζ ZORA-def2-TZVP[97,98] basis set for all atoms with $Z \leq 36$ and the SARC-ZORA-TZVP[99–101] basis set for all atoms with $Z > 36$. For PBE0, the calculations were also done without ZORA applying the def2-TZVP[97] basis set with the def2 effective core potentials (ECP).[102,103] For the NMR shielding calculations in Sections 3.4.2 and 3.4.3, the CPCM[104] implicit solvation model was used. All calculations applied the RI scheme with the chain-of-spheres approximation for the exchange (RIJCOSX)[105,106] in combination with the auxiliary SARC/J basis set. The defgrid3 grid and the tightscf convergence settings were used throughout. For the high-level reference values (ADF), the NMR shielding calculations were performed each with the scalar (SR) and spin–orbit (SO) variant of ZORA[40,107,108] and the PBE0 functional using the STO polarized triple-ζ ZORA/TZ2P[63] basis set (the "ZORA/" prefix for the basis set is from now assumed for all calculations with ADF and omitted for clarity). The numerical grid quality was set to verygood. For the compounds of the methyl subset, the same calculation settings were applied, but with using the DZ, DZP, TZP, and QZ4P basis sets[63] and the PBE, BLYP,[109,110] mPW,[111] B3LYP,[110,112] and mPW1PW[111] functionals.

In the ML training, prediction, and evaluation procedures mentioned in the following, statistical fluctuations are to be expected that originate from the randomized weight initialization when the model is build. All statistics presented for the performance of the $\Delta_{SO}$-ML model are therefore obtained as the mean value of ten training runs if not stated otherwise.

## 3 Results

### 3.1 Prediction of $\Delta_{SO}\delta$ for ¹³C NMR

Before focusing on the new $\Delta_{SO}$-ML correction, it is worth investigating the data set itself with the computed low-level SR NMR shifts and the reference $\Delta_{SO}\delta$ values. As a rather short-range effect, the SO contribution is expected to be small for many C/H atoms, but can be extreme in direct vicinity of a heavy atom. The complete data for the ¹³C NMR shifts is depicted in Fig. 3(b) including information about the chemical distance (= number of covalent bonds) of each nucleus to the next heavy atom. Thus, ¹³C nuclei that are directly bound to a HA experience by far the largest spin–orbit coupling effects and these values are most scattered over a wide range of chemical shifts. Still, the SO effect of a HA can propagate which can have
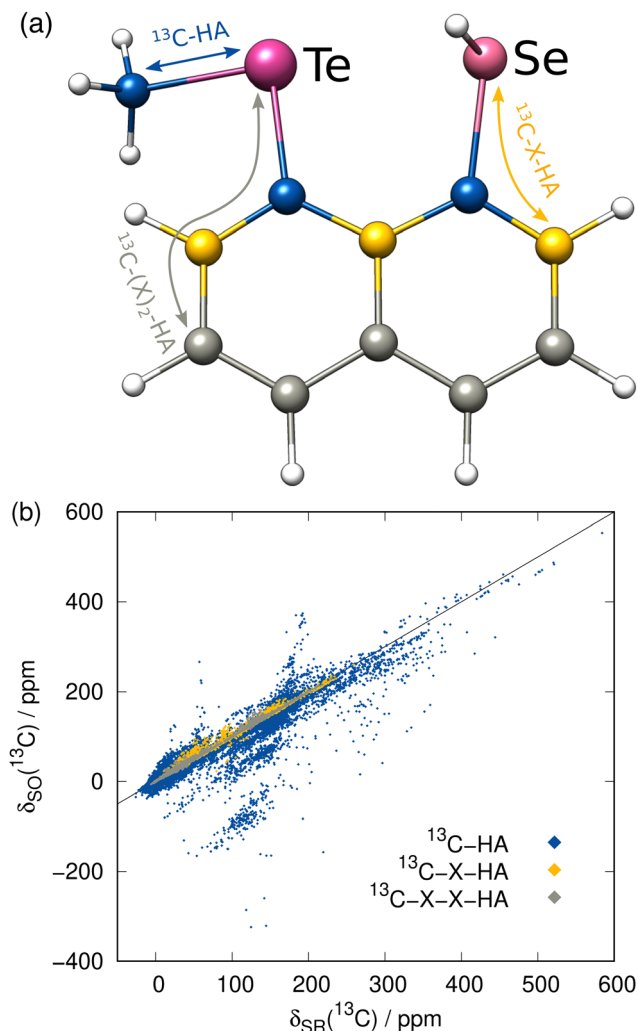
This journal is © the Owner Societies 2024

*Phys. Chem. Chem. Phys.*, 2024, **26**, 4870–4884 | **4873**

**Fig. 3** (a) Example molecule (part of the data set) showing the division of the $^{13}$C data set into three distance categories with one (blue), two (yellow), and three or more (gray) bonds between the HA and the $^{13}$C nucleus (H atoms are white). (b) Complete data set with 38 740 $^{13}$C NMR chemical shifts showing the relation between the purely scalar-relativistic NMR shift $\delta_{SR}$ calculated with the low-level PBE0/ZORA-def2-TZVP method and the relativistic reference $\delta_{SO} = \delta_{SR} + \Delta_{SO}\delta$ with the SO contribution calculated at the PBE0/TZ2P level.

**Table 1** Statistics of the test data set before and after applying the $\Delta_{SO}$-ML correction to the scalar-relativistic (SR) baseline SR-PBE0/def2-TZVP values in ppm (MSD in ppm$^2$), reference: SO-PBE0/TZ2P. Mean over ten training runs, more details on the metrics are given in the ESI

| Error metric | $^{13}$C | | $^1$H | |
| --- | --- | --- | --- | --- |
| | Only SR | SR + ML | Only SR | SR + ML |
| MAX ($<0$) | −179.07 | −56.34 | −19.569 | −4.772 |
| MAX ($>0$) | 298.32 | 87.55 | 6.042 | 10.825 |
| MD | 2.84 | −0.05 | −0.185 | −0.005 |
| MAD | 7.26 | 1.07 | 0.281 | 0.090 |
| MSD | 478.82 | 7.60 | 0.645 | 0.056 |
| RMSD | 21.88 | 2.76 | 0.803 | 0.236 |
| SD | 21.67 | 2.75 | 0.782 | 0.236 |

accuracy. The mean absolute deviation (MAD) from 4843 chemical shifts in the test data set (unknown to the ML model while training) is reduced by 85% from 7.26 to 1.07 ppm and the mean (signed) deviation (MD), which is slightly positive when only SR is applied, essentially reaches zero. More importantly, the root mean square deviation (RMSD), which emphasizes large deviations, is equally reduced (87%, from 21.88 to 2.76 ppm). Thus, it can be concluded that roughly 85% of the SO contribution is recovered by the ML model. Analysis of one of the training runs in Fig. 4(a) shows that accuracy is maintained even for the extreme cases of spin–orbit coupling effects on $^{13}$C nuclei directly bound to HAs. The large negative values of $\Delta_{SO}\delta$ occur especially when several heavy halogen atoms are present, such as in a $CI_3$ moiety.

Furthermore, extremely large errors can be avoided with the $\Delta_{SO}$-ML correction as the maximum negative and positive errors are reduced drastically from −179.07/+298.32 to −56.34/+87.55 ppm. This is promising because in this way the ML correction reduces the probability of a complete qualitative failure of a chemical shift prediction. The overall chance for outliers is therefore reduced significantly as underpinned by Fig. 4(b).

It is important to note that an empirical prediction method for spin–orbit effects to NMR chemical shifts is not a straightforward task. It is indeed a rather systematic phenomenon as it strongly depends on the type and the atomic number of the HA as well as the periodic table main group it belongs to. So, when the underlying data only features a certain chemical subgroup of molecules, a simple linear regression approach, which is often used to correct calculated NMR chemical shifts and which we used to compare the performance of the $\Delta_{corr}$-ML model to, can be used to approximate the SO contribution to $^{13}$C NMR chemical shifts.[113,114] However, this is only possible if all molecules in the data set contain the same number and type of heavy atoms.[13] Conversely, in the data set presented here, many different HAs and amounts of HAs are present and therefore, there is not even a slight linear connection between the computed scalar-relativistic chemical shift value and the missing SO contribution (see the ESI,† Fig. S3 to S5). Hence, a linear regression correction approach fails for the SO contribution, as it predicts $\Delta_{SO}\delta \approx 0$ in most cases. However, the additional computational costs of a prediction of $\Delta_{SO}\delta$ by the a pre-trained ML model is – as for the linear regression

significant consequences for the $^{13}$C nuclei even three covalent bonds away. Although the nuclei closest to the HA have the potential to lead to the largest errors in a calculation, the proposed ML model should not only be capable of reproducing the rough magnitude of the effect, but should consequently predict a small $\Delta_{SO}\delta$ value for the weakly affected nuclei.

As mentioned earlier, the PBE0/ZORA-def2-TZVP method applying scalar-relativistic SR-ZORA is chosen as low-level method for the following investigations. Several metrics demonstrating the performance of the $\Delta_{SO}$-ML model evaluated for the test data set (12.5% of the data points) for $^{13}$C and $^1$H (discussed in the next section) nuclei are listed in Table 1. The data for one of the runs is exemplarily shown in Fig. 4 in more detail.

The $\Delta_{SO}$-ML correction clearly succeeds to predict the SO contribution to the $^{13}$C NMR chemical shifts with good

**4874** | *Phys. Chem. Chem. Phys.*, 2024, **26**, 4870–4884

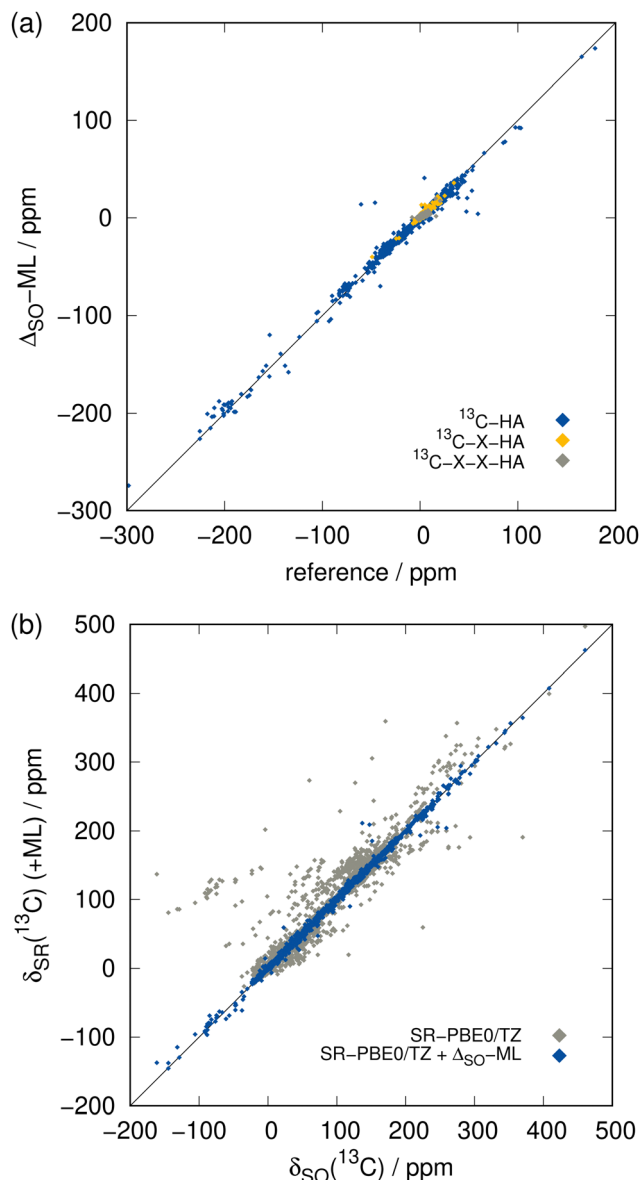This journal is © the Owner Societies 2024

Fig. 4 Comparison of the ML-predicted SO contributions to the reference (SR/SO)-ZORA-PBE0/TZ2P ones for the $^{13}$C NMR test set. (a) Values of $\Delta_{SO}\delta$, color-coded according to their distance to the next heavy atom (see Fig. 3(a)). (b) Total chemical shift $\delta$ neglecting SO coupling (gray) and adding the ML-predicted $\Delta_{SO}\delta$ (blue).

approach – negligible (few seconds). This consolidates the significance of the $\Delta_{SO}$-ML model as a general low-cost method to predict the SO contribution of NMR chemical shifts.

### 3.2 Prediction of $\Delta_{SO}\delta$ for $^1$H NMR

The focus of this work lies on the prediction of SO contributions to $^{13}$C NMR chemical shifts since in organic compounds, usually the carbon atoms are connected to heavy heteroatoms. However, the $^1$H nucleus can experience SO contributions from even further HAs as it is more prone to environmental changes and thus can be affected by propagation of the SO contribution *via* more than three covalent bonds. Compared to heavier elements, the hydrogen atom only comprises a very thin

electron shell and the $^1$H nucleus is thus less shielded from electronic and magnetic fields in its surroundings. This complicates especially the theoretical description of core properties such as NMR parameters. Achieving the same accuracy for $^1$H NMR as for $^{13}$C NMR is therefore difficult, which we already observed for the $\Delta_{corr}$-ML correction and there is no reason to assume that this behavior is different in the case of $\Delta_{SO}$-ML. This is even exacerbated by the fact that the hydrogen atoms are usually further away from the HA than carbon atoms meaning that the $\Delta_{SO}\delta$ values are smaller and can be less systematic. The data set for $^1$H NMR SO contributions shows a significant number of large values not only for very close $^1$H nuclei, but
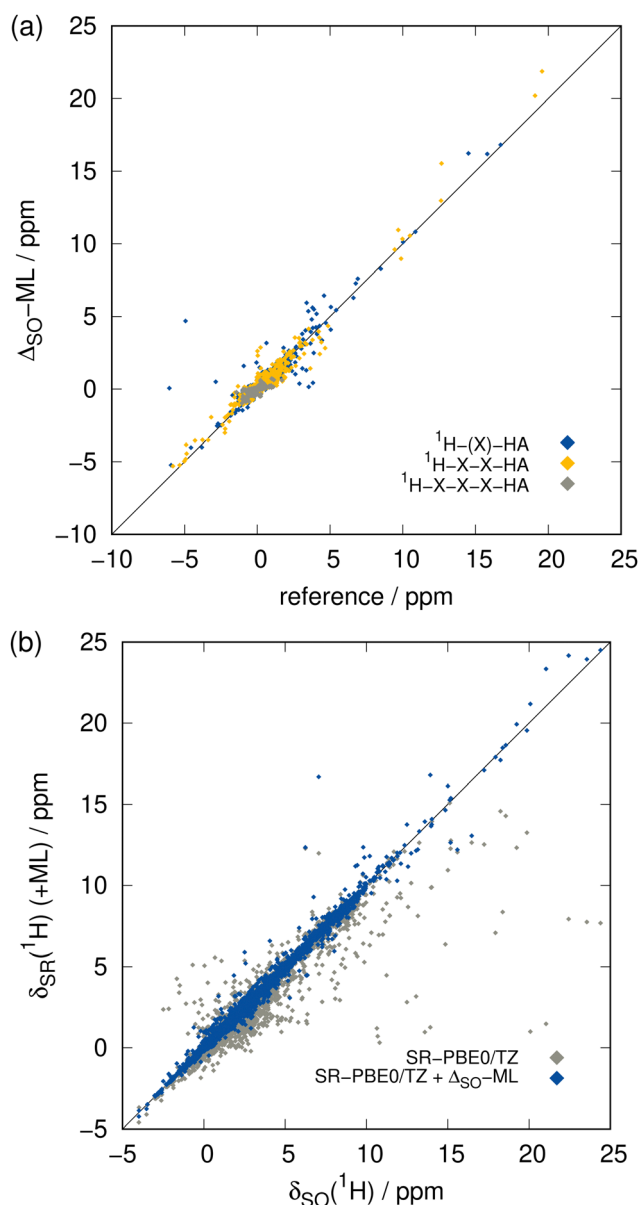


Fig. 5 Comparison of the ML-predicted SO contributions to the reference (SR/SO)-ZORA-PBE0/TZ2P ones for the $^1$H NMR test set. (a) Values of $\Delta_{SO}\delta$, color-coding: $^1$H bound to a HA directly or *via* two (blue), three (yellow), or four or more (gray) covalent bonds. (b) Total chemical shift $\delta$ neglecting SO coupling (gray) and adding the ML-predicted $\Delta_{SO}\delta$ (blue).

This journal is © the Owner Societies 2024

*Phys. Chem. Chem. Phys.*, 2024, **26**, 4870–4884 | **4875**

also for those bound to a HA *via* three covalent bonds (see ESI,† Fig. S2). Hence, the distance criterion is weaker for $^1$H than it is for $^{13}$C, representing a bigger challenge for the $\Delta_{SO}$-ML model.

The greater complexity compared to $^{13}$C NMR is confirmed by the somewhat weaker performance of the $\Delta_{SO}$-ML approach applied to the low-level method SR-PBE0/ZORA-def2-TZVP for $^1$H NMR indicated by the metrics in Table 1 and the detailed analysis of a training run in Fig. 5. Compared to the $^{13}$C data, the performance of the ML approach for $^1$H NMR is indeed worse, but the functionality is still retained. The $\Delta_{SO}$-ML method predicts qualitatively correct values within the whole data range even in the extreme regions (Fig. 5(a)) and scattering of the data including the ML-predicted SO contributions is reduced significantly compared to the purely SR values (Fig. 5(b)). It is noticeable that the data of nuclei in close and medium vicinity to a HA is spread over the whole data range, only the $^1$H nuclei at least four bonds away from the HA are loosely restricted to a region of small $\Delta_{SO}\delta$ values and small prediction errors. The overall improvement achieved by the correction is also substantiated by the metrics in Table 1. That is, the MAD resulting from the 8055 data points in the test set is reduced by 68% from 0.281 to 0.090 ppm and the overall chance for large errors is reduced, too, as indicated by the 71% decrease of the RMSD from 0.803 to 0.236 ppm. In contrast to the $^{13}$C NMR case, the MD for the purely SR $^1$H NMR chemical shifts is slightly negative, but it is nevertheless basically eliminated. Unfortunately, there is at least one large outlier in the predicted $\Delta_{SO}\delta$ values leading to an increased positive maximum error of 10.825 ppm. Taking into account the overall reduced error spread and range (reduced from 26.611 to 15.597 ppm) as well as the small RMSD, this can be considered an artifact that occurs only very rarely.

The fundamental non-linear correlation between the scalar-relativistic NMR chemical shift and its missing spin–orbit coupling contribution seems to be general and can at least be transferred form $^{13}$C to $^1$H NMR (see ESI,† Fig. S6 to S8). The linear regression technique is therefore unusable also for the $^1$H NMR case. To conclude, despite the lower performance of the $\Delta_{SO}$-ML approach for $^1$H compared to $^{13}$C NMR, it still accomplishes a decent improvement, especially if the negligible extra computational expenses and efforts are considered.

### 3.3 Generalizability of the model

#### 3.3.1 Method dependence of $\Delta_{SO}\delta$.
Since the presented prediction method is supposed to be generally valid, it would be beneficial if the spin–orbit contribution to the chemical shift $\Delta_{SO}\delta$ calculated with DFT does not depend strongly on the functional and basis set that are used for its computation. This can be expected due to the "doubly relative" nature of $\Delta_{SO}\delta$ ($\delta$: difference between two shielding constants, $\Delta$: difference between SR and SO). To test this dependence, a small test set called methyl subset, which is also included in the ML data set, has been investigated with different DFT levels of theory. It contains compounds of all heavy atoms saturated with methyl groups (except for the halogens), more precisely, the molecules $CH_3A^I$, $CHA^I_3$, $(CH_3)_2A^{II}$, $(CH_3)_3A^{III}$, and $(CH_3)_4A^{IV}$ (with $A^I = Cl$,

**Table 2** Deviation in ppm of $\Delta_{SO}\delta$ calculated with various functional/basis set combinations evaluated to the reference level of theory PBE0/TZ2P on the methyl subset of compounds. M(A)D = Mean (absolute) deviation

| Functional | Basis set | $^{13}$C | | $^1$H | |
|---|---|---|---|---|---|
| | | MD | MAD | MD | MAD |
| PBE0 | DZ | −1.28 | 1.28 | 0.022 | 0.045 |
| PBE0 | DZP | −0.60 | 0.64 | 0.016 | 0.025 |
| PBE0 | TZP | −0.28 | 0.40 | 0.006 | 0.012 |
| PBE0 | QZ4P | 0.11 | 0.30 | 0.003 | 0.013 |
| PBE | TZ2P | −0.82 | 0.84 | 0.004 | 0.053 |
| BLYP | TZ2P | −1.74 | 1.98 | 0.012 | 0.065 |
| mPW | TZ2P | −0.94 | 0.94 | 0.000 | 0.063 |
| B3LYP | TZ2P | −1.05 | 1.51 | 0.010 | 0.019 |
| mPW1PW | TZ2P | −0.12 | 0.26 | −0.003 | 0.006 |
| PBE0 | TZ2P | 0.00 | 0.00 | 0.000 | 0.000 |

Br, I; $A^{II}$ = Zn, Cd, Hg, Se, Te; $A^{III}$ = Ga, In, Tl, As, Sb, Bi; $A^{IV}$ = Ge, Sn, Pb). As mentioned earlier, the PBE0/TZ2P level of theory was chosen for the calculation of the reference $\Delta_{SO}\delta$ values. The average deviations of those from other functionals and basis sets are summarized in Table 2. In all test molecules, all carbon nuclei are in direct vicinity to the HA, and all hydrogen nuclei are connected to the HA *via* two covalent bonds.

Variation of the basis set size is found to have an almost negligible effect on $\Delta_{SO}\delta$ when still a triple- or quadruple-$\zeta$ size is sustained with maximum mean absolute deviations of 0.40 ppm for $^{13}$C (TZP) and 0.013 ppm for $^1$H (QZ4P). These values lie below the typically expected errors for density functional approximations (DFA) of roughly 3–8 ppm for $^{13}$C NMR and 0.1–0.3 ppm for $^1$H NMR.[6] When the basis set size is reduced to double-$\zeta$ (DZ, DZP), significantly larger deviations are observed. Therefore, TZ2P is considered a well-balanced and reasonably large basis set for the purpose of this work. The use of different DFAs exhibits a more pronounced effect on the value of $\Delta_{SO}\delta$. While for $^{13}$C, no dependence on the functional class (GGA/hybrid) is observed, in the $^1$H case, the deviation from the hybrid PBE0 to the GGAs is larger than for the hybrids DFAs. Nevertheless, even when BLYP is used, which has the largest MAD compared to PBE0 (1.98 ppm for $^{13}$C, 0.65 ppm for $^1$H), the functional differences are still very low. According to these data, the SO prediction method is expected to be generalizable to methods other than PBE0/TZ2P with a small residual method inconsistency error.

#### 3.3.2 Transferability of the $\Delta_{SO}$-ML method.
The claim made earlier, that the reference $\Delta_{SO}\delta$ contribution can basically be predicted *via* any low-level DFT method, has yet to be proven. Therefore, three other example DFT levels of theory were investigated regarding their use as baseline methods for the $\Delta_{SO}$-ML approach. These include SR-ZORA in conjunction with PBE as the GGA variant in the same functional family as PBE0 and r$^2$SCAN0 as a different hybrid DFA that performed well for both $^1$H and $^{13}$C NMR chemical shifts with respect to canonical CCSD(T) evaluated on the data set of the $\Delta_{corr}$-ML model.[55] Furthermore, an approach without the explicit treatment of scalar-relativistic effects is investigated, namely PBE0/def2-TZVP, which uses the def2 effective core potentials (ECP) for elements with $Z > 36$ and thus implicitly comprises some

**4876** | *Phys. Chem. Chem. Phys.*, 2024, **26**, 4870–4884

This journal is © the Owner Societies 2024

amount of relativity. Furthermore, the question arises whether it is necessary to recompute all chemical shifts of the data set and retrain the $\Delta_{SO}$-ML model if methods other than SR-PBE0 are used.

Answers to these questions can be obtained from analyzing the performance differences of the mentioned methods for the test data set depicted in Fig. 6. First, the previously examined performance using the SR-PBE0 method is clearly visible when compared to the *uncorrected* data (without any SO contribution) and the prediction qualities for all other tested methods are of equal dimension. By taking a closer look, it is surprising to find that in the case of $^{13}C$ NMR, the performance of the $\Delta_{SO}$-ML method is not reduced noticeably when SR-PBE or SR-r$^2$SCAN0

are used as low-level methods. This means that the electronic and magnetic input features obtained from PBE and r$^2$SCAN0 chemical shielding calculations closely resemble those from a PBE0 calculation (all geometric descriptors are identical). A computationally more affordable level of theory such as PBE can therefore easily be used to reconstruct the SO contribution to the $^{13}C$ NMR chemical shift at the PBE0 level without changing the ML model. Subsequently, it is not surprising that the $\Delta_{SO}$-ML approaches for PBE and r$^2$SCAN0 retain their performance when the model is trained on data obtained from these respective DFAs. The situation changes slightly, when not the functional, but the relativistic approximation is changed. The use of the simpler ECP variant of PBE0/def2-TZVP
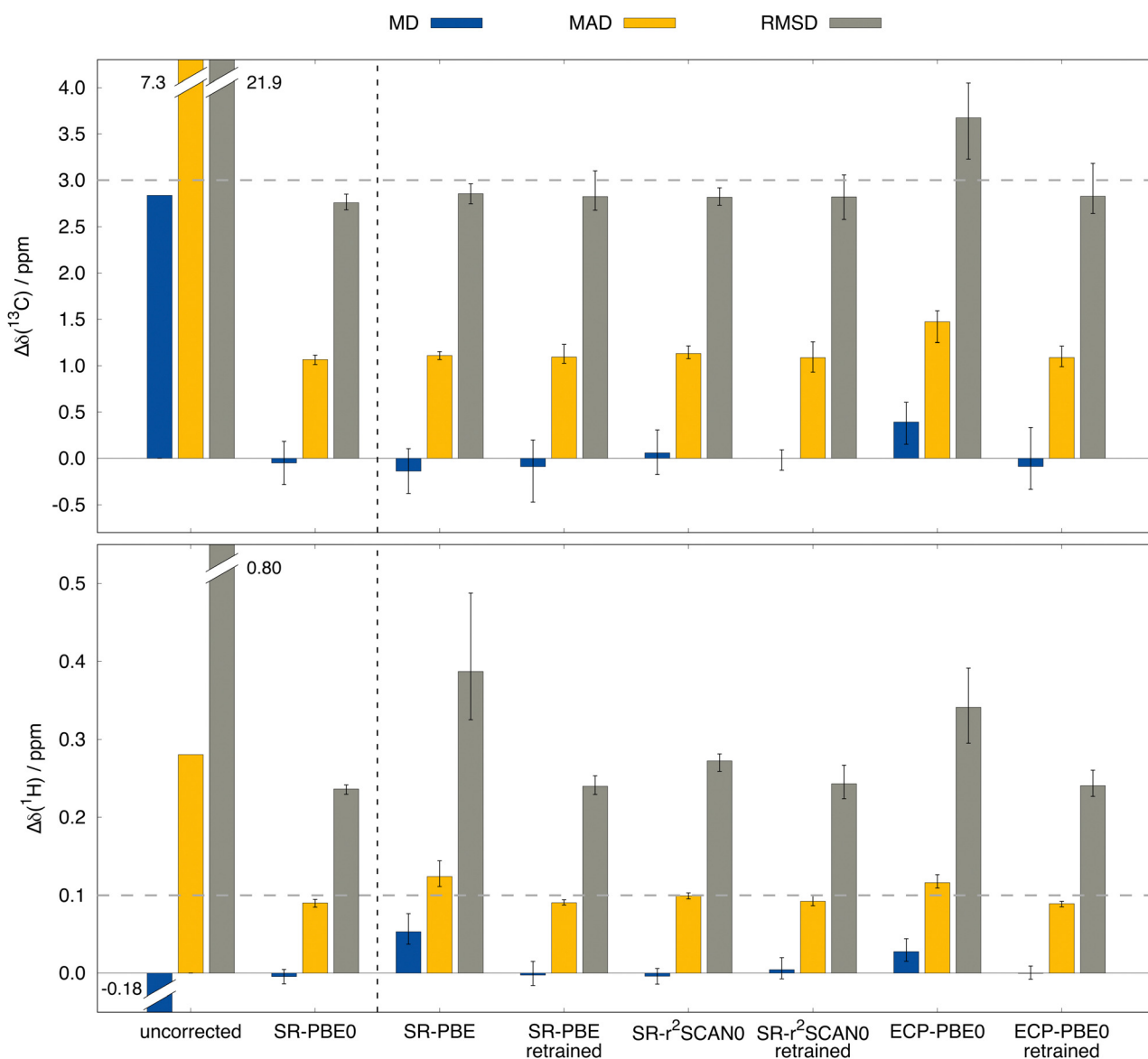


Fig. 6 Comparison of different low-level methods as baseline of the $\Delta_{SO}$-ML approach and their metrics evaluated for the $^{13}C$ and $^1H$ test data sets. In all cases, the def2-TZVP basis set in the scalar-relativistic ZORA (SR) framework or with the def2-ECPs (ECP) has been used with the respective functional, uncorrected refers to $\Delta_{SO}\delta = 0$. Each functional's data results from using the ML model trained on SR-PBE0 data, while *retrained* indicates that the ML model has been recreated using the training data calculated at the respective level of theory. The horizontal dashed line indicates the minimum expectable DFT method error.

This journal is © the Owner Societies 2024

*Phys. Chem. Chem. Phys.*, 2024, **26**, 4870–4884 | **4877**

and the standard instead of the ZORA Hamiltonian results in a slightly increased RMSD of 3.67 ppm (compared to 2.76 ppm for SR-PBE0/ZORA-def2-TZVP) and a larger error spread. This indicates that the input features differ more severely between the ECP and SR-ZORA approaches than between the different functionals. For some further insights, a selection of six electronic and magnetic $^{13}$C descriptors is depicted in Fig. 7 showing their correlation when obtained from the different calculations *via* the ECP and the SR-ZORA approach. In all cases, a more or less strongly pronounced correlation is found which explains the ability of the $\Delta_{SO}$-ML method to predict reasonable results even without retraining of the model. Since the correlation has an approximately linear character, the ML model is capable of adapting to the different data when it is retrained and thus recovers its initial performance (RMSD of 2.83 ppm). The features from the ECP-PBE0 calculation are therefore not necessarily less suited for use in the ML model.

Analysis of the results for $^1$H NMR reveals the expected behavior for the more complex circumstances mentioned above. In contrast to $^{13}$C, there are significant performance losses if other functionals are used to generate the ML input features. While the initial RMSD of 0.236 ppm for SR-PBE0/ZORA-def2-TZVP is only slightly increased to 0.272 ppm for SR-r$^2$SCAN0, the loss is more drastic for SR-PBE with an RMSD of 0.387 ppm, which is even

higher than the RMSD of ECP-PBE0 (0.341 ppm). Apparently, the $^1$H nucleus is more prone to differences in the input features and the variations between data from different functionals is larger than for $^{13}$C NMR. This might, to some extent, originate from the much smaller typical chemical shift range for $^1$H NMR (about 0–12 ppm) for which deviations of a few tenths of ppm are already substantial. Nonetheless, also for $^1$H NMR the performance of the original SR-PBE0 method can be recovered when the model is trained on the corresponding data. Thus, RMSDs of 0.240, 0.243, and 0.241 ppm can be achieved for SR-PBE, SR-r$^2$SCAN0, and ECP-PBE0, respectively. Despite the limited number of investigated DFT levels of theory, we feel confident that the presented behaviour of the $\Delta_{SO}$-ML method is of general nature, making it a powerful tool for the low-cost assessment of SO contributions to computed NMR chemical shifts. Even when the base method SR-PBE0 cannot be applied, the $\Delta_{SO}\delta$ values predicted from lower-level DFT methods are reliable enough for a rough estimation and can serve as diagnostic tool to detect possible severe SO contributions and avoid large computational errors.

### 3.4 Performance for external test systems

To evaluate the $\Delta_{SO}$-ML method in real-world applications, it was tested on three different sets that are independent from the
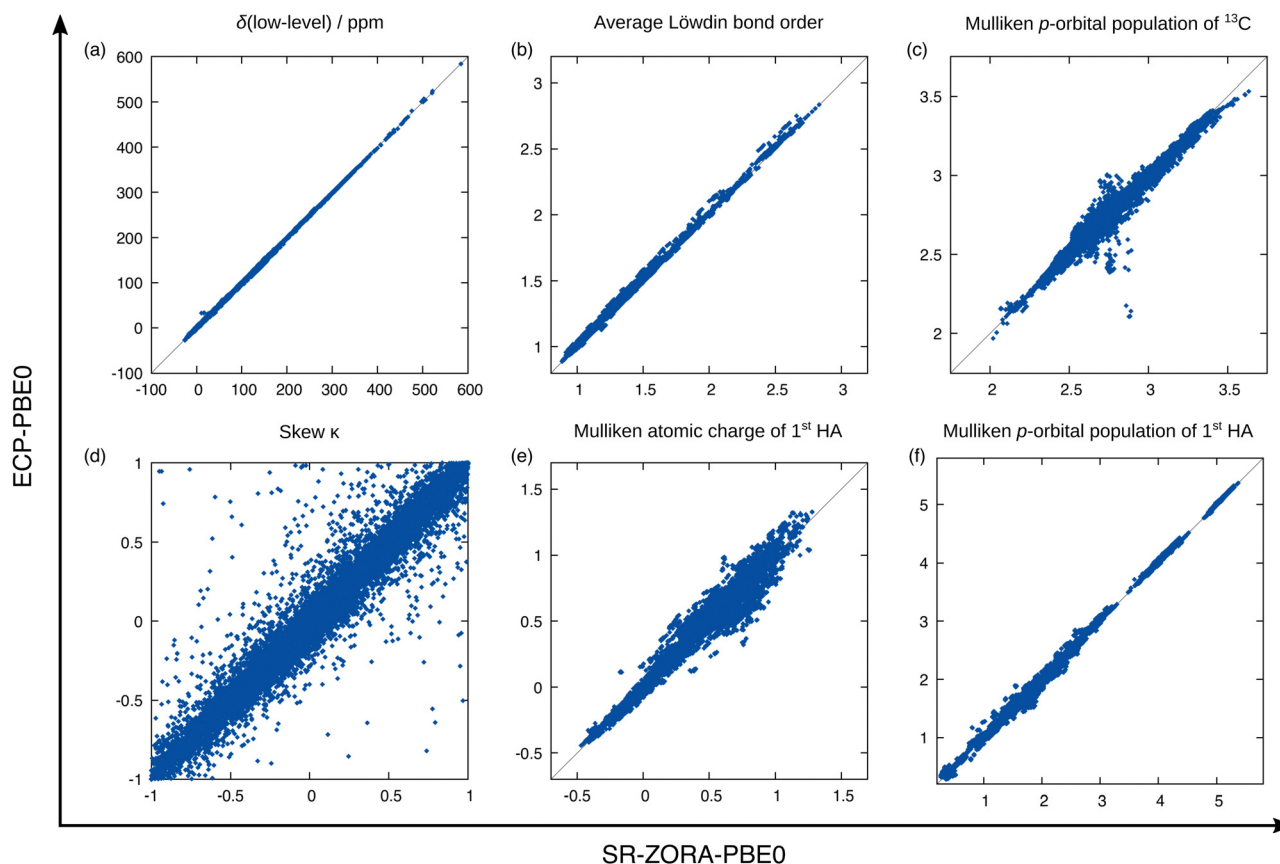


**Fig. 7** Correlation plots of a selection of descriptors in the $^{13}$C input feature vector as calculated at the PBE0 level with the ECP variant (def2-TZVP) against the SR-ZORA variant (ZORA-def2-TZVP). (a) $\delta$ calculated at low-level, (b) average bond order of all bonds of the respective $^{13}$C, (c) p-orbital population at the $^{13}$C, (d) skew $\kappa = \dfrac{3(\sigma_{iso} - \sigma_{22})}{\sigma_{33} - \sigma_{11}}$ (from shielding tensor $\sigma$), (e) atomic charge of the neighboring HA, (f) p-orbital (valence) population of the neighboring HA.

data set used for training and testing described herein. These are the SnS51[11] set containing various organotin compounds and its successor for organolead chemistry[115] (Section 3.4.1). In addition, a new set has been compiled for HALA effects on $^{13}C$ nuclei comprising experimental $^{13}C$ NMR chemical shifts from structures with all 17 heavy elements included in the training data of the $\Delta_{SO}$-ML method, which we call 17HAC (Section 3.4.2). Finally, the particularly difficult example of a bismabenzene compound is showcased in more detail (Section 3.4.3).

**3.4.1 Performance for organotin and organolead compounds.** In comprehensive benchmark studies, we investigated various DFT methods regarding their ability to predict $^{119}Sn$ and $^{207}Pb$ NMR chemical shifts. Most of the compounds from these studies were now used to investigate the HALA effect caused by the presence of Sn/Pb atoms and the predictive power of the $\Delta_{SO}$-ML approach on this quantity. For this purpose, the conformers lowest in Gibbs free energy from both benchmark sets were recalculated at the reference level of theory used herein (SO-ZORA-PBE0/TZ2P) for a purely computational evaluation (for more technical details, see the ESI,† Section 3.2.1). Thus, a data set containing 817 $^{13}C$ NMR chemical shifts in Sn-containing compounds and 1415 in Pb-containing compounds (for $^1H$ NMR: 1170 and 2059, respectively) was analyzed.

The results for $^{13}C$ NMR are shown in Fig. 8 and segmented into subgroups of atoms with different distances between the heavy and the light atom. It is obvious that in both cases (Sn and Pb), the (virtually costless) $\Delta_{SO}$-ML prediction helps to reduce the relativity-related errors drastically. It stands out that this is especially significant for $^{13}C$ nuclei directly bound to the HA, which is the clear strength of the method. In the case of organolead compounds, this category undergoes the by far most pronounced HALA effects (RMSD of 29.55 ppm if no SO contribution is included). For $^{13}C$ nuclei connected to Pb via more than one bond, the initial errors are much smaller due to a notably smaller SO contribution making it more difficult to cover the effect by the correction method. For a distance of three or more bonds, $\Delta_{SO}$-ML does not yield a useful prediction anymore, which, in practice, would not stand out as the average SO contribution of this category (MAD of 2.21 ppm) is below the typical error of DFT in general. The analysis of the organotin compounds suggests a very similar behavior with the main difference that the SO contribution form Sn as HA is generally smaller. Still, the $\Delta_{SO}$-ML method predicts large SO contributions reasonably well and also improved the overall statistics, but the generally smaller $\Delta_{SO}\delta$ values are lost in the DFT-related noise sooner.

Similar trends are observed for the $^1H$ NMR data, whereas a more pronounced HALA effect on nuclei connected to Sn/Pb via two and three bonds was noticed (see Fig. S9 in the ESI†). However, the overall SO contributions are again significantly smaller so that the $\Delta_{SO}$-ML correction will be less important than the choice of an appropriate density functional in these cases. Nevertheless, it succeeds in predicting large SO contributions in $^1H$ nuclei close to Pb atoms.
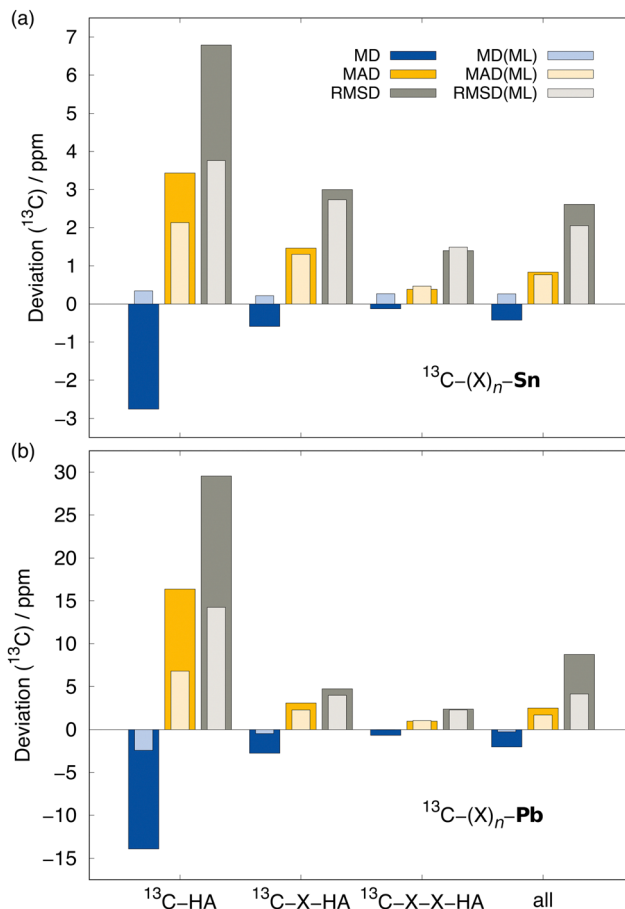


**Fig. 8** Comparison of $^{13}C$ NMR metrics for the (a) C–Sn and (b) C–Pb test structures without any SO contribution (PBE0/ZORA-def2-TZVP, full colors) and with the ML-predicted $\Delta_{SO}\delta$ values (brighter colors). The data is averaged over $^{13}C$ nuclei bound to a HA via one (C–HA), two (C–X–HA), and three or more bonds (C–X–X–HA) and over the full data (all).

**3.4.2 Performance on the 17HAC test set.** When heavy elements are involved, it is obvious that any inclusion of SO contributions to chemical shifts should reduce the deviation to experimental data. However, we have so far only tested the $\Delta_{SO}$-ML approach with respect to theoretical reference data. As it is important to validate the method against experimental data, too, a new benchmark set was constructed that consists of 63 mostly organic molecules featuring all 17 HAs (at least three molecules per heavy element) included in the training data set. In total, 236 experimental $^{13}C$ NMR shifts were collected from nuclei in different distances form the HA and with different degrees of SO effects to the $^{13}C$ nucleus (more details are given in the ESI,† Section 3.2.2). To systematically address all typical sources of error mentioned in the beginning, the following workflow was applied for all compounds. First, a conformer search was performed as described in Section 2.4 to integrate the conformational flexibility of the systems. The plain DFT results were then obtained as the Boltzmann-average of the $^{13}C$ NMR chemical shifts calculated with PBE0/ZORA-def2-TZVP with the implicit CPCM solvent model to incorporate solvent effects. Subsequently, in order to tackle the electron correlation

This journal is © the Owner Societies 2024

*Phys. Chem. Chem. Phys.*, 2024, **26**, 4870–4884 | **4879**

and relativistic effects to the NMR shifts, the $\Delta_{SO}$-ML and $\Delta_{corr}$-ML (retrained on *low-level* PBE0/ZORA-def2-TZVP data) corrections were applied to calculations without a solvent model and the contributions were added. The last main error source – the rotational-vibrational effects – are expected to mostly cancel when chemical shifts are calculated relative to a reference compound.[116] Some exemplary results from this workflow are shown in Fig. 9 and the final statistics are given in Table 3.

The analysis in Table 3 shows that the two $\Delta$-ML corrections tackle different quantities. Upon including the SO effects *via* $\Delta_{SO}$-ML, the RMSD is reduced drastically, because the focus of the correction lies in detecting large SO-HALA effects which leads to a clear decrease of the large errors in these cases. On the other hand, the $\Delta_{corr}$-ML corrects for a rather systematic correlation-related error which is usually not as large for single cases, but smaller, yet significant, for the majority of the ^{13}C nuclei. Therefore, the RMSD is only slightly reduced, but the MAD is smaller than when only $\Delta_{SO}$-ML is used. Nevertheless, the best results are achieved when both corrections are applied, yielding a roughly halved value for all statistical quantities (MAD reduced by 50%, RMSD by 55%). Hence, a systematic treatment of the typical error sources in the computation of NMR chemical shifts does lead to a systematic decrease of the deviation to experimental data.

**3.4.3 Showcase: bismabenzene.** For the majority of the test cases shown so far, the nuclei (especially ^{13}C) closest to the HA were affected most by spin–orbit effects. However, the effect is

**Table 3** Statistics for the 17HAC benchmark set evaluated with the baseline PBE0/ZORA-def2-TZVP(CPCM) level (SR) and with systematic addition of the ML-predicted spin–orbit and/or correlation contributions

| Error metric | SR | $+\Delta_{SO}$-ML | $+\Delta_{corr}$-ML | +Both |
|---|---|---|---|---|
| MAX ($<0$) | −37.32 | −15.75 | −50.38 | −18.47 |
| MAX ($>0$) | 112.62 | 73.11 | 104.58 | 61.54 |
| MD | 9.99 | 8.59 | 6.33 | 4.94 |
| MAD | 11.41 | 8.93 | 8.81 | 5.73 |
| RMSD | 20.81 | 12.48 | 18.80 | 9.37 |

able to propagate[33] and in rare cases, it can even be much larger for atoms further away. This seems to be the case in bismabenzene, where the Bi–[13]C effect is largest in the *para* position. We therefore studied a bismabenzene derivative that could be synthesized[117] in order to test the $\Delta_{SO}$-ML method for a representative extreme case with only little similar data available for training. As before, a conformer ensemble was generated and refined at the r[2]SCAN-3c level of theory and solvation was included applying CPCM (chloroform). The reference SO contributions are depicted in Fig. 10 and the results are listed in Table 4.

Most importantly, the extreme $\Delta_{SO}\delta$ value of the *para*-^{13}C needs to be included in order to achieve a qualitative agreement with the experiment (*i.e.*, $\delta$(^{13}C,*meta*) $<$ $\delta$(^{13}C,*para*)). Furthermore, despite being visibly too low for *para*-^{13}C, the predicted $\Delta_{SO}\delta$ values are in qualitative agreement with the reference method. Including both ML contributions (SO and corr) does not recover the correct ordering of the chemical shifts, but significantly approaches the experimental results. A similar behavior is observed for ^{1}H NMR with the *meta*-^{1}H being affected most. Since a satisfying agreeing is not achieved even with including both the true SO contribution and the ML-predicted correlation correction, we attribute the major part of the remaining error to solvation and dynamic effects. Nevertheless, the example of the bismabenzene compound shows that the $\Delta_{SO}$-ML method provides reasonable approximations to the SO contribution to NMR chemical shifts even in potentially unexpected cases.
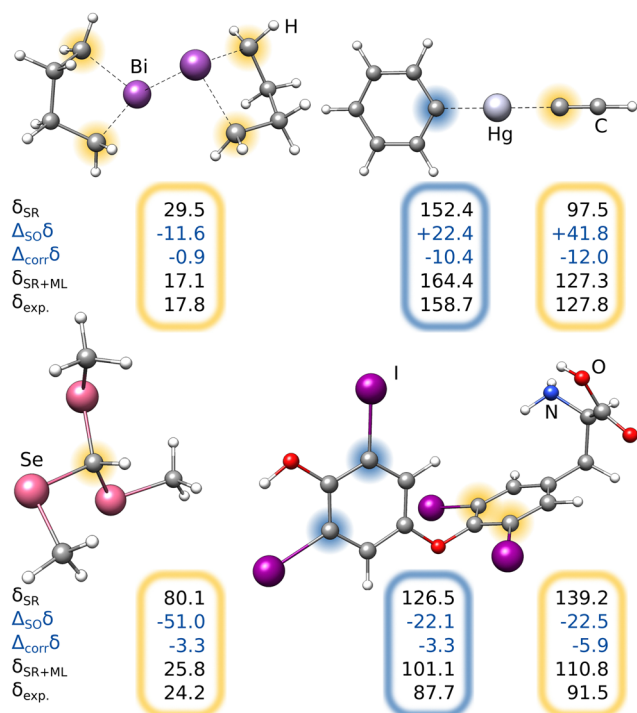


**Fig. 9** Four example molecules from the 17HAC test set (showing the lowest-energy conformer) and selected ^{13}C NMR chemical shifts calculated with the low-level DFT method PBE0/ZORA-def2-TZVP before (SR) and after addition of the $\Delta$-ML contributions (SR + ML) and compared to experimental values.
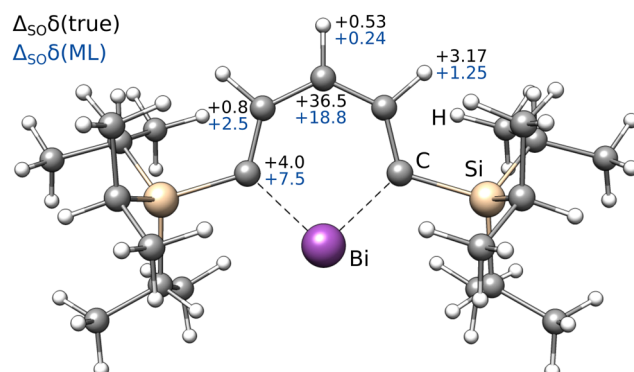


**Fig. 10** Lowest conformer of the investigated bismabenzene derivative and $\Delta_{SO}\delta$ values given in ppm for the aromatic ^{13}C and ^{1}H nuclei as calculated at the SO-ZORA-PBE0/TZ2P level of theory (true, black) or predicted *via* the $\Delta_{SO}$-ML method (blue) and Boltzmann-weighted over all conformers.

4880 | *Phys. Chem. Chem. Phys.*, 2024, **26**, 4870–4884

This journal is © the Owner Societies 2024

**Table 4** Chemical shift data for the investigated bismabenzene derivative calculated with the low-level method (SR-PBE0/ZORA-def2-TZVP) and the spin−orbit (SO) and correlation (corr) contributions resulting in total values with both contributions predicted with ML (ML/ML) or using the true SO contribution (true/ML). All chemical shift values are Boltzmann-averaged and include a solvation contribution from CPCM

| | $^{13}$C | | | $^1$H | |
| --- | --- | --- | --- | --- | --- |
| | ortho | meta | para | meta | para |
| Low-level | 241.5 | 147.3 | 121.9 | 8.93 | 7.57 |
| $\Delta_{SO}\delta$ (ML) | +7.5 | +2.5 | +18.8 | +1.25 | +0.24 |
| $\Delta_{SO}\delta$ (true) | +4.0 | +0.8 | +36.5 | +3.17 | +0.53 |
| $\Delta_{corr}\delta$ (ML) | −13.7 | −2.9 | −4.4 | −0.25 | −0.15 |
| Total (ML/ML) | 235.2 | 147.0 | 136.3 | 9.93 | 7.66 |
| Total (true/ML) | 231.8 | 145.2 | 153.9 | 11.85 | 7.95 |
| Experiment | 222.4 | 136.5 | 153.5 | 11.62 | 7.68 |

For the lowest-energy conformer of the bismabenzene derivative, timing evaluations were performed at different theory levels (see Fig. 11). While several hours are required using the all-electron SR low-level methods (*e.g.*, PBE0/ZORA-def2-TZVP), the SO reference calculation takes multiple days. In contrast, the training of the $\Delta_{SO}$-ML model lasts a few minutes (for ten training runs for statistical averaging) and the prediction of $\Delta_{SO}\delta$ is done in seconds on a usual desktop computer. The speed advantage of the presented method is thus evident and it is emphasized that using an ECP-based low-level method has the potential of an even larger speedup with a comparable performance of the $\Delta_{SO}$-ML method.

# 4 Conclusion

The consideration of relativistic spin–orbit effects for molecules containing heavy atoms is vital for the reliable simulation of their $^{13}$C and $^1$H NMR spectra. This treatment is computationally much more demanding than a non-relativistic calculation and requires non-standard procedures and software, making it less accessible for non-expert users and unsuitable for screening purposes. We presented a machine learning regression-based approach called $\Delta_{SO}$-ML to approximate the
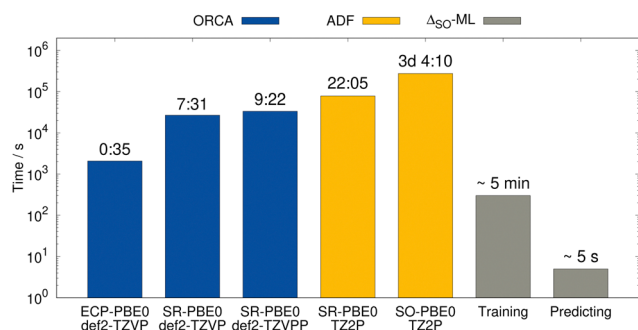


**Fig. 11** Timings for NMR shielding calculations of the bismabenzene derivative at different DFT levels (ORCA) compared with SR and SO calculations (ADF) and the time required by the $\Delta_{SO}$-ML model. Calculations were performed in parallel on four cores of an Intel Xeon CPU E3-1270 v5 @ 3.60 GHz. Values in hours:min; the ML evaluations were performed on a usual desktop PC.

SO contribution in $^{13}$C and $^1$H NMR chemical shifts. The underlying data set contains 6388 structures with 17 of the most important heavy elements from group 12 to 17 and NMR calculations at a hybrid DFT level including SO-relativistic treatment *via* the ZORA technique for 38 740 $^{13}$C and 64 436 $^1$H NMR chemical shifts. Moreover, the data set can easily be extended by including more diverse structures, *e.g.*, with total charges or further heavy atoms. We showed that the method recovers about 85% of the SO contribution for $^{13}$C (70% for $^1$H) on the test data subset. It is further transferable for use with other density functionals than the base method PBE0 and other approaches for including scalar-relativistic effects, such as ECPs. Since the SO contribution $\Delta_{SO}\delta$ depends only slightly on the DFA and basis set as shown for heavy atom methyl compounds, the generalizability of the $\Delta_{SO}$-ML method renders it broadly applicable for a wide range of DFT methods with a fairly good accuracy even without retraining the model for other low-level methods. In principle, it is not even limited to DFT, but only needs a method that can provide the required input features. This might be correlated methods such as coupled cluster or semiempirical approaches. Predicting $\Delta_{SO}\delta$ is done in a few seconds and only requires the converged low-level NMR shielding calculation and the pre-trained ML model, making it superior to other low-cost methods such as linear regression techniques, that are only applicable to special problems.

Off its training and test data set, the method proved powerful for the prediction of SO contributions caused by nearby Sn and Pb atoms in realistic systems. Moreover, a workflow that systematically addresses all main error sources in NMR parameter computation significantly reduces the deviations to experimental data throughout all 17 HAs resulting in an average error reduction by about 50% when both the $\Delta_{SO}$- and $\Delta_{corr}$-ML corrections are applied. If the computational resources allow an explicit treatment of the SO-relativistic effects, the $\Delta_{SO}$-ML method can function as a diagnostic prescreening tool to identify systems with potentially large SO contributions that are subsequently treated on a higher level of theory only if necessary. The potential fields of application of the $\Delta_{SO}$-ML method lie in high-throughput workflows such as structure assignment methods that can be improved when a higher level of theory is used[118] and as an additional ingredient in low-cost composite method approaches that rarely include any relativistic treatment.[119] To conclude, the new $\Delta_{SO}$-ML method is able to robustly predict SO contributions to NMR chemical shifts for large systems and delivers its full potential when used together with the $\Delta_{corr}$-ML correction in low-cost NMR prediction schemes.

## Data availability statement

The implementation of the $\Delta_{SO}$-ML and $\Delta_{corr}$-ML methods as well as the associated data sets can be found at **https://github.com/grimme-lab/ml4nmr**.

## Conflicts of interest

There are no conflicts to declare.

This journal is © the Owner Societies 2024

*Phys. Chem. Chem. Phys.*, 2024, **26**, 4870–4884 | **4881**

# Acknowledgements

# Notes and references

1  A.-H. Emwas, R. Roy, R. T. McKay, L. Tenori, E. Saccenti, G. A. Nagana Gowda, D. Raftery, F. Alahmari, L. Jaremko, M. Jaremko and D. S. Wishart, *Metabolites*, 2019, **9**, 123.

2  D. J. Kubicki, S. D. Stranks, C. P. Grey and L. Emsley, *Nat. Rev. Chem.*, 2021, **5**, 624–645.

3  I. Speciale, A. Notaro, P. Garcia-Vello, F. Di Lorenzo, S. Armiento, A. Molinaro, R. Marchetti, A. Silipo and C. De Castro, *Carbohydr. Polym.*, 2022, **277**, 118885.

4  C. van Wüllen, in *Calculation of NMR and EPR Parameters*, ed. M. Kaupp, M. Bühl and V. G. Malkin, Wiley-VCH, Weinheim, 2004, ch. 6, pp. 83–100.

5  A. M. Teale, O. B. Lutnæs, T. Helgaker, D. J. Tozer and J. Gauss, *J. Chem. Phys.*, 2013, **138**, 024111.

6  D. Flaig, M. Maurer, M. Hanni, K. Braunger, L. Kick, M. Thubauville and C. Ochsenfeld, *J. Chem. Theory Comput.*, 2014, **10**, 572–578.

7  C. van Wüllen, *Phys. Chem. Chem. Phys.*, 2000, **2**, 2137–2144.

8  C. J. Schattenberg and M. Kaupp, *J. Chem. Theory Comput.*, 2021, **17**, 7602–7621.

9  C. J. Schattenberg, M. Lehmann, M. Bühl and M. Kaupp, *J. Chem. Theory Comput.*, 2022, **18**, 273–292.

10  M. Bursch, T. Gasevic, J. B. Stückrath and S. Grimme, *Inorg. Chem.*, 2021, **60**, 272–285.

11  J. B. Stückrath, T. Gasevic, M. Bursch and S. Grimme, *Inorg. Chem.*, 2022, **61**, 3903–3917.

12  G. L. Stoychev, A. A. Auer and F. Neese, *J. Chem. Theory Comput.*, 2018, **14**, 4756–4771.

13  M. W. Lodewyk, M. R. Siebert and D. J. Tantillo, *Chem. Rev.*, 2012, **112**, 1839–1862.

14  L. B. Krivdin, *Magn. Reson. Chem.*, 2019, **57**, 897–914.

15  L. B. Krivdin, *Prog. Nucl. Magn. Reson. Spectrosc.*, 2019, **112–113**, 103–156.

16  Z. Zhang, J. Zhu, S. Chen, W. Sun and D. Wang, *Angew. Chem., Int. Ed.*, 2023, **62**, e202215136.

17  K. Chen, Y. Zhang, J. Xiang, X. Zhao, X. Li and K. Chu, *ACS Energy Lett.*, 2023, **8**, 1281–1288.

18  H. W. Moon and J. Cornella, *ACS Catal.*, 2022, **12**, 1382–1393.

19  K. Guan, L. Tao, R. Yang, H. Zhang, N. Wang, H. Wan, J. Cui, J. Zhang, H. Wang and H. Wang, *Adv. Energy Mater.*, 2022, **12**, 2103557.

20  C. Xiao, W. Song, J. Liang, J. Zhang, Z. Huang, J. Zhang, H. Wang, C. Zhong, J. Ding and W. Hu, *J. Mater. Chem. A*, 2022, **10**, 3667–3677.

21  H. Dong, C. Ran, W. Gao, N. Sun, X. Liu, Y. Xia, Y. Chen and W. Huang, *Adv. Energy Mater.*, 2022, **12**, 2102213.

22  J. S. Kim, J.-M. Heo, G.-S. Park, S.-J. Woo, C. Cho, H. J. Yun, D.-H. Kim, J. Park, S.-C. Lee, S.-H. Park, E. Yoon, N. C. Greenham and T.-W. Lee, *Nature*, 2022, **611**, 688–694.

23  W. Koch, M. Czop, K. Ilowiecka, A. Nawrocka and D. Wiacek, *Nutrients*, 2022, **14**, 1626.

24  N. Natasha, M. Shahid, I. Bibi, J. Iqbal, S. Khalid, B. Murtaza, H. F. Bakhat, A. B. U. Farooq, M. Amjad, H. M. Hammad, N. K. Niazi and M. Arshad, *Sci. Total Environ.*, 2022, **808**, 152024.

25  S. Ruangritchankul, C. Sumananusorn, J. Sirivarasai, W. Monsuwan and P. Sritara, *Nutrients*, 2023, **15**, 322.

26  E. Scarpellini, L. M. Balsiger, V. Maurizi, E. Rinninella, A. Gasbarrini, N. Giostra, P. Santori, L. Abenavoli and C. Rasetti, *BioFactors*, 2022, **48**, 294–306.

27  X. Zheng, B. Ren, X. Li, H. Yan, Q. Xie, H. Liu, J. Zhou, J. Tian and K. Huang, *J. Biol. Inorg. Chem.*, 2020, **25**, 1009–1022.

28  M. Schwarz, C. E. Meyer, A. Löser, K. Lossow, J. Hackler, C. Ott, S. Jäger, I. Mohr, E. A. Eklund, A. A. H. Patel, N. Gul, S. Alvarez, I. Altinonder, C. Wiel, M. Maares, H. Haase, A. Härtlova, T. Grune, M. B. Schulze, T. Schwerdtle, U. Merle, H. Zischka, V. I. Sayin, L. Schomburg and A. P. Kipp, *Nat. Commun.*, 2023, **14**, 3479.

29  I. A. Gallardo, D. A. Todd, S. T. Lima, J. R. Chekan, N. H. Chiu and E. W. Taylor, *Antioxidants*, 2023, **12**, 559.

30  T. B. Demissie, *J. Chem. Phys.*, 2017, **147**, 174301.

31  S. Moncho and J. Autschbach, *J. Chem. Theory Comput.*, 2010, **6**, 223–234.

32  Y. Y. Rusakov, I. L. Rusakova and L. B. Krivdin, *Int. J. Quantum Chem.*, 2016, **116**, 1404–1412.

33  J. Vícha, J. Novotný, S. Komorovsky, M. Straka, M. Kaupp and R. Marek, *Chem. Rev.*, 2020, **120**, 7065–7103.

34  B. A. Hess, *Phys. Rev. A: At., Mol., Opt. Phys.*, 1986, **33**, 3742–3748.

35  G. Jansen and B. A. Hess, *Phys. Rev. A: At., Mol., Opt. Phys.*, 1989, **39**, 6016–6017.

36  W. Kutzelnigg and W. Liu, *J. Chem. Phys.*, 2005, **123**, 241102.

37  M. Iliaš and T. Saue, *J. Chem. Phys.*, 2007, **126**, 064102.

38  D. Peng, W. Liu, Y. Xiao and L. Cheng, *J. Chem. Phys.*, 2007, **127**, 104106.

39  E. van Lenthe, E. J. Baerends and J. G. Snijders, *J. Chem. Phys.*, 1993, **99**, 4597–4610.

40  E. van Lenthe, J. G. Snijders and E. J. Baerends, *J. Chem. Phys.*, 1996, **105**, 6505–6516.

41  D. L. Crittenden, *Phys. Chem. Chem. Phys.*, 2022, **24**, 27055–27063.

42  A. G. Kutateladze and D. S. Reddy, *J. Org. Chem.*, 2017, **82**, 3368–3381.

43  J. S. Smith, O. Isayev and A. E. Roitberg, *Chem. Sci.*, 2017, **8**, 3192–3203.

44  T. Zubatiuk, B. Nebgen, N. Lubbers, J. S. Smith, R. Zubatyuk, G. Zhou, C. Koh, K. Barros, O. Isayev and S. Tretiak, *J. Chem. Phys.*, 2021, **154**, 244108.

**4882** | *Phys. Chem. Chem. Phys.*, 2024, **26**, 4870–4884

This journal is © the Owner Societies 2024

45 D. M. Anstine, R. Zubatyuk and O. Isayev, *ChemRxiv*, 2023, preprint, DOI: 10.26434/chemrxiv-2023-296ch.

46 D. Chen, Z. Wang, D. Guo, V. Orekhov and X. Qu, *Chem. Eur. J.*, 2020, **26**, 10391–10401.

47 A. Gupta, S. Chakraborty and R. Ramakrishnan, *Mach. Learn.: Sci. Technol.*, 2021, **2**, 035010.

48 S. K. Chandy and K. Raghavachari, *J. Chem. Theory Comput.*, 2023, **19**, 6632–6642.

49 S. G. Smith and J. M. Goodman, *J. Am. Chem. Soc.*, 2010, **132**, 12946–12959.

50 A. Howarth, K. Ermanis and J. M. Goodman, *Chem. Sci.*, 2020, **11**, 4351–4359.

51 M. M. Zanardi and A. M. Sarotti, *J. Org. Chem.*, 2015, **80**, 9371–9378.

52 M. Ruth, D. Gerbig and P. R. Schreiner, *J. Chem. Theory Comput.*, 2023, **19**, 4912–4920.

53 P. Gao, J. Zhang, Q. Peng, J. Zhang and V.-A. Glezakou, *J. Chem. Inf. Model.*, 2020, **60**, 3746–3754.

54 P. A. Unzueta, C. S. Greenwell and G. J. O. Beran, *J. Chem. Theory Comput.*, 2021, **17**, 826–840.

55 J. B. Kleine Büning and S. Grimme, *J. Chem. Theory Comput.*, 2023, **19**, 3601–3615.

56 J. Li, J. Liang, Z. Wang, A. L. Ptaszek, X. Liu, B. Ganoe, M. Head-Gordon and T. Head-Gordon, *arXiv*, 2023, preprint, arXiv:2306.08269, https://arxiv.org/abs/2306.08269v1.

57 A. Bagno and G. Saielli, *Theor. Chem. Acc.*, 2007, **117**, 603–619.

58 T. E. Field-Theodore, M. Olejniczak, M. Jaszunski and D. J. D. Wilson, *Phys. Chem. Chem. Phys.*, 2018, **20**, 23025–23033.

59 A. Bagno, F. Rastrelli and G. Saielli, *J. Phys. Chem. A*, 2003, **107**, 9964–9973.

60 S. Grimme, A. Hansen, S. Ehlert and J. M. Mewes, *J. Chem. Phys.*, 2021, **154**, 064103.

61 C. Adamo and V. Barone, *J. Chem. Phys.*, 1999, **110**, 6158–6170.

62 C. Adamo and V. Barone, *Chem. Phys. Lett.*, 1998, **298**, 113–119.

63 E. Van Lenthe and E. J. Baerends, *J. Comput. Chem.*, 2003, **24**, 1142–1156.

64 E. Heid, C. J. McGill, F. H. Vermeire and W. H. Green, *J. Chem. Inf. Model.*, 2023, **63**, 4012–4029.

65 J. Behler, *J. Chem. Phys.*, 2011, **134**, 074106.

66 C. Bannwarth, S. Ehlert and S. Grimme, *J. Chem. Theory Comput.*, 2019, **15**, 1652–1671.

67 xTB - Semiempirical Extended Tight-Binding Program Package, Version 6.6.0, Universität Bonn, Mulliken Center for Theoretical Chemistry, Bonn, Germany 2023, https://github.com/grimme-lab/xtb/releases/.

68 TURBOMOLE, Version 7.7.1, Universität Karlsruhe & Forschungszentrum Karlsruhe GmbH, Karlsruhe, Germany 2023, https://www.turbomole.org/.

69 F. Furche, R. Ahlrichs, C. Hättig, W. Klopper, M. Sierka and F. Weigend, *WIREs Comput. Mol. Sci.*, 2014, **4**, 91–100.

70 S. G. Balasubramani, G. P. Chen, S. Coriani, M. Diedenhofen, M. S. Frank, Y. J. Franzke, F. Furche, R. Grotjahn, M. E. Harding, C. Hättig, A. Hellweg, B. Helmich-Paris, C. Holzer, U. Huniar, M. Kaupp, A. Marefat Khah, S. Karbalaei Khani, T. Müller, F. Mack, B. D. Nguyen, S. M. Parker, E. Perlt, D. Rappoport, K. Reiter, S. Roy, M. Rückert, G. Schmitz, M. Sierka, E. Tapavicza, D. P. Tew, C. van Wüllen, V. K. Voora, F. Weigend, A. Wodynski and J. M. Yu, *J. Chem. Phys.*, 2020, **152**, 184107.

71 J. W. Furness, A. D. Kaplan, J. Ning, J. P. Perdew and J. Sun, *J. Phys. Chem. Lett.*, 2020, **11**, 8208–8215.

72 E. Caldeweyher, C. Bannwarth and S. Grimme, *J. Chem. Phys.*, 2017, **147**, 034112.

73 K. Eichkorn, O. Treutler, H. Öhm, M. Häser and R. Ahlrichs, *Chem. Phys. Lett.*, 1995, **240**, 283–290.

74 P. Pracht, F. Bohle and S. Grimme, *Phys. Chem. Chem. Phys.*, 2020, **22**, 7169–7192.

75 CREST - Conformer-Rotamer Ensemble Sampling Tool, Version 2.12, Universität Bonn, Mulliken Center for Theoretical Chemistry, Bonn, Germany 2022, https://github.com/crest-lab/crest/releases/.

76 S. Spicher and S. Grimme, *Angew. Chem., Int. Ed.*, 2020, **59**, 15665–15673.

77 S. Ehlert, M. Stahn, S. Spicher and S. Grimme, *J. Chem. Theory Comput.*, 2021, **17**, 4250–4261.

78 S. Grimme, F. Bohle, A. Hansen, P. Pracht, S. Spicher and M. Stahn, *J. Phys. Chem. A*, 2021, **125**, 4039–4054.

79 CENSO - Commandline Energetic Sorting of Conformer-Rotamer Ensembles, Version 1.2.0, Universität Bonn, Mulliken Center for Theoretical Chemistry, Bonn, Germany 2022, https://github.com/grimme-lab/censo/releases/.

80 A. Klamt, *J. Phys. Chem.*, 1995, **99**, 2224–2235.

81 A. Klamt, V. Jonas, T. Bürger and J. C. W. Lohrenz, *J. Phys. Chem. A*, 1998, **102**, 5074–5085.

82 F. Eckert and A. Klamt, *AIChE J.*, 2002, **48**, 369–385.

83 S. Grimme, *Chem. – Eur. J.*, 2012, **18**, 9955–9964.

84 S. Spicher and S. Grimme, *J. Phys. Chem. Lett.*, 2020, **11**, 6606–6611.

85 S. Spicher and S. Grimme, *J. Chem. Theory Comput.*, 2021, **17**, 1701–1714.

86 S. Sinnecker, A. Rajendran, A. Klamt, M. Diedenhofen and F. Neese, *J. Phys. Chem. A*, 2006, **110**, 2235–2245.

87 R. Ditchfield, *Mol. Phys.*, 1974, **27**, 789–807.

88 K. Wolinski, J. F. Hinton and P. Pulay, *J. Am. Chem. Soc.*, 1990, **112**, 8251–8260.

89 G. Schreckenbach and T. Ziegler, *J. Phys. Chem.*, 1995, **99**, 606–611.

90 ORCA - An ab initio, DFT and semiempirical SCF-MO package, Version 5.0.4, Max-Planck-Institut für Kohlenforschung, Mülheim a. d. Ruhr, Germany 2022, https://www.faccts.de/orca/.

91 F. Neese, *WIREs Comput. Mol. Sci.*, 2012, **2**, 73–78.

92 F. Neese, *WIREs Comput. Mol. Sci.*, 2022, 1–15.

93 AMS - Amsterdam Modeling Suite, Version 2022.103, SCM, Vrije Universiteit, Amsterdam, The Netherlands 2022, https://www.scm.com/amsterdam-modeling-suite/.

94 S. K. Wolff, T. Ziegler, E. van Lenthe and E. J. Baerends, *J. Chem. Phys.*, 1999, **110**, 7689–7698.

This journal is © the Owner Societies 2024

*Phys. Chem. Chem. Phys.*, 2024, **26**, 4870–4884 | 4883

95 J. P. Perdew, K. Burke and M. Ernzerhof, *Phys. Rev. Lett.*, 1996, **77**, 3865–3868.

96 M. Bursch, H. Neugebauer, S. Ehlert and S. Grimme, *J. Chem. Phys.*, 2022, **156**, 134105.

97 F. Weigend and R. Ahlrichs, *Phys. Chem. Chem. Phys.*, 2005, **7**, 3297–3305.

98 R. Ahlrichs and K. May, *Phys. Chem. Chem. Phys.*, 2000, **2**, 943–945.

99 D. A. Pantazis, X.-Y. Chen, C. R. Landis and F. Neese, *J. Chem. Theory Comput.*, 2008, **4**, 908–919.

100 D. A. Pantazis and F. Neese, *Theor. Chem. Acc.*, 2012, **131**, 1292.

101 J. D. Rolfes, F. Neese and D. A. Pantazis, *J. Comput. Chem.*, 2020, **41**, 1842–1849.

102 D. Andrae, U. Häußermann, M. Dolg, H. Stoll and H. Preuß, *Theor. Chim. Acta*, 1990, **77**, 123–141.

103 K. A. Peterson, D. Figgen, E. Goll, H. Stoll and M. Dolg, *J. Chem. Phys.*, 2003, **119**, 11113–11123.

104 V. Barone and M. Cossi, *J. Phys. Chem. A*, 1998, **102**, 1995–2001.

105 F. Neese, F. Wennmohs, A. Hansen and U. Becker, *Chem. Phys.*, 2009, **356**, 98–109.

106 G. L. Stoychev, A. A. Auer, R. Izsák and F. Neese, *J. Chem. Theory Comput.*, 2018, **14**, 619–637.

107 E. van Lenthe, E. J. Baerends and J. G. Snijders, *J. Chem. Phys.*, 1994, **101**, 9783–9792.

108 M. Krykunov, T. Ziegler and E. van Lenthe, *Int. J. Quantum Chem.*, 2009, **109**, 1676–1683.

109 A. D. Becke, *Phys. Rev. A: At., Mol., Opt. Phys.*, 1988, **38**, 3098–3100.

110 C. Lee, W. Yang and R. G. Parr, *Phys. Rev. B: Condens. Matter Mater. Phys.*, 1988, **37**, 785–789.

111 C. Adamo and V. Barone, *J. Chem. Phys.*, 1998, **108**, 664–675.

112 P. J. Stephens, F. J. Devlin, C. F. Chabalowski and M. J. Frisch, *J. Phys. Chem.*, 1994, **98**, 11623–11627.

113 D. J. Giesen and N. Zumbulyadis, *Phys. Chem. Chem. Phys.*, 2002, **4**, 5498–5507.

114 P. dAntuono, E. Botek, B. Champagne, M. Spassova and P. Denkova, *J. Chem. Phys.*, 2006, **125**, 144309.

115 *Manuscript in preparation*.

116 A. A. Auer, J. Gauss and J. F. Stanton, *J. Chem. Phys.*, 2003, **118**, 10407–10417.

117 T. Ishii, K. Suzuki, T. Nakamura and M. Yamashita, *J. Am. Chem. Soc.*, 2016, **138**, 12787–12790.

118 N. Grimblat, M. M. Zanardi and A. M. Sarotti, *J. Org. Chem.*, 2015, **80**, 12526–12534.

119 J. Liang, Z. Wang, J. Li, J. Wong, X. Liu, B. Ganoe, T. Head-Gordon and M. Head-Gordon, *J. Chem. Theory Comput.*, 2023, **19**, 514–523.

**4884** | *Phys. Chem. Chem. Phys.*, 2024, **26**, 4870–4884

This journal is © the Owner Societies 2024